Sol-gel transition in porous media

Interplay of drying and wetting

le Dizes, R.

Publication date
2024

2

Is unidirectional drying in a round capillary always diffusive? *

The unidirectional drying of water in cylindrical capillaries has been described since Stefan's solution as a vapor diffusion controlled process with a square root of time kinetics. Here we show that this well-known process actually depends on the way the capillary is closed. Experiments are performed on the evaporation of water in capillaries closed at one end with a solid material or connected to a fluid reservoir. While we recover Stefan's solution in the first case, we show that in the second situation the water plug evaporates at a constant rate with the water-air meniscus remaining pinned at the exit where evaporation proceeds. The presence of the liquid reservoir closing the capillary combined with a capillary pumping effect induces a flow of the water plug toward the evaporation front leading to a constant-rate drying, substantially faster than the prediction of Stefan's equation. Our results show that a transition from a constant-rate evaporation regime at short times to a diffusion-driven evaporation regime at long times can be observed by increasing the viscosity of the fluid in the reservoir blocking the other end of the capillary. Such transition can also be observed by connecting the capillary end to a solidifying fluid like epoxy glue.

* *This chapter is based on:* R. Le Dizès Castell, M. Prat, S. Jabbari-Farouji and N. Shahidzadeh *Is unidirectional drying in a round capillary always diffusive ?*, Langmuir. 39, 5462–5468, **2023**

2.1 Introduction

Understanding the drying processes of porous media is of major importance for soils in agriculture[105], civil engineering, petrophysics or the conservation of stone artworks[106] and has been the subject of many studies. However, the accurate prediction of the evaporation rate from a porous medium remains a challenge[107,108]. As discussed in Chapter 1, modeling of flow through porous materials is often based on the concept of considering the pore network as a bundle of parallel cylindrical tubes with varying diameters[109,110]. A capillary can also be considered as the elementary unit in pore network models[63], an approach that has proven to be an effective way to gain meaningful insights into the transport and drying properties of porous media[111]. In other words, the consideration of a single capillary is both interesting for highlighting the physics at pore scale and in the prospect of scale bridging via pore network or lattice Boltzmann models[112] for instance.

Stefan[75] in 1871 was the first to describe the diffusion-driven drying in a vertical capillary tube: he showed that the evaporation of a liquid in a circular tube slows down as the air-liquid interface is receding inside the tube[76]. Since then, round capillaries have been used in several studies to understand the flow and transport processes with different fluids such as ionic solutions[77,113] or colloidal suspensions[114]. Unidirectional drying in capillaries has also been extensively studied by changing different parameters including geometry and wettability properties of capillaries.[78,115,116] But most of the previous studies focus on unidirectional drying in fully saturated capillaries and closed by a solid phase (glass or epoxy glue for instance). But in nature, drying of a porous medium can happen in a lot of different configurations. For instance, during evaporation, the initially liquid-filled pores are gradually occupied by gas: this gas invasion leads to disconnections in the liquid pathway to the surface thus creating discontinuous water flows[116]. Drying can therefore happen in dead-end and two open-end pores but also in pores connected to a supply in water. It can be also noticed that the consideration of tubes or channels with two open ends is classical in the studies of drying of colloidal suspensions.[114,117,118]

Here we show that the classical description of unidirectional drying in capillaries used as model pores depends on the closing condition of the capillary. While drying in cylindrical capillaries closed by a solid plug follows a classical diffusion driven behaviour, a faster capillary drying regime, characterized by a constant-rate period[60,119], can be induced when the capillary end is in contact with a liquid plug. This case is similar to the constant-rate period (CRP) observed within porous media[60,119] although drying of a single capillary cannot be representative of all the mechanisms explaining the CRP observed with porous media[108]. In the case of porous media, the CRP is notably due to the fact that many pores remain saturated at the surface as the result of the preferential invasion of the coarser pores. In the case of a single tube, the CRP is obtained because the

meniscus stays pinned at the tube end, somewhat similar to the situation of finer pores in a porous medium. More generally, the present study can be seen as a contribution to the current trend of addressing drying in situations of greater complexity[74,77,113,114,117,118] than the classical drying problems with a pure liquid.

2.2 Methods

We used in this study round and square borosilicate glass capillaries purchased from VitroCom, cut to a length of roughly 20 mm (of inner diameter $d = 0.5$ mm and wall thickness $w = 0.1$ mm for round capillaries and of width 0.5 mm, wall thickness $w = 0.1$ mm for square capillaries). The capillaries are cleaned with ethanol and demineralised water and dried for 24h at 60°C. The unidirectional drying is subsequently investigated in two situations as illustrated in Fig. 2.1-a and b.

a) Capillaries closed by a solid plug: One end of the capillary is melted with a torch prior to the filling with water. Once melted, an ultra-thin Pasteur pipette is used to partially fill the capillary with demineralised water ($V_0 \approx 0.6$ μL). A gas plug is therefore present in between the melted end and the entraped volume of water evaporating.

b) Capillaries connected to a liquid plug: The capillary is partially filled with demineralised water (by capillary suction $V_0 \approx 0.6 - 1$ μL) and placed horizontally. A big droplet of liquid (roughly 2 mL) is deposited at the other end of the capillary opposite to the entrapped volume of water evaporating. Here again, some air remains trapped inside the capillary between the entrapped water evaporating from the open side and the large droplet of liquid (here defined as fluid A) closing the other end of the capillary. The volume of the latter is maintained roughly constant during the experiment. The impact of the viscosity of fluid A on the kinetics of the drying of water plugs are investigated by using different liquids as fluid A: demineralised water, glycerol (Sigma Aldrich) and PDMS 100000 cSt (Sigma Aldrich). Finally, in some experiments, nail polish purchased from Etos and epoxy glue purchased from Liquimoly are used as fluid A to close the capillaries.

These two configurations can be seen as pore scale configurations corresponding to the drying situation (configuration (a) and the evaporation-wicking situation (configuration (b)) in porous media studies[120].

All the experiments are performed horizontally to avoid the effect of gravity. The evaporation of the entrapped water inside the capillary is monitored using an inverted Leica DM IRM microscope with a 2.5 magnification objective for both configurations. An image is taken every 10 seconds until the end of the drying. The relative humidity is measured for each experiment using a Testo 645 thermo-hygrometer. The temperature is kept at 20°C.

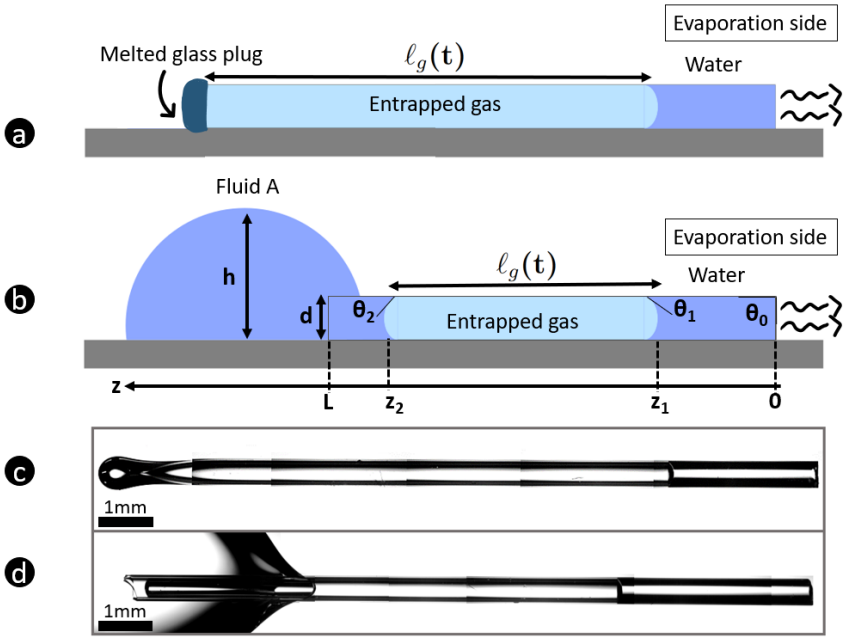

Figure 2.1. Schematics and pictures of unidirectional drying in round capillaries for the two studied configurations. In configuration (a), the left end of the capillary is melted whereas in configuration (b) the capillary is closed by a liquid droplet deposited at the left end. Panels (c) and (d) are microscopy images of configurations (a) and (b) at the start of the experiment $t = 0$. The evaporating water corresponds to the blue shaded zone on the right side of the images.

2.3 Results

2.3.1 Different drying regimes

The results for the two configurations are shown in Fig. 2.2, where the ratio of the volume of entrapped water at the time t relative to its initial value is plotted as a function of time. Surprisingly, we observe two different drying behaviors for the capillaries with a melted end (configuration (a)) and those connected to a liquid reservoir (configuration (b)). In situation (a), where one end of the capillary is melted (solid plug), the water meniscus on the evaporation side of the capillary starts receding inside the capillary immediately. The water meniscus on the closed side of the capillary (position z_1 in Fig. 2.1) remains in place and does not move during drying. Consequently the volume of the gas plug V_g (entrapped gas in Fig. 2.1) remains constant. On the contrary in configuration (b), the water meniscus on the evaporation side remains almost pinned at the exit during the drying and the evaporation rate is constant. Water thus evaporates substantially faster compared to situation (a).

In case (a) as the bulk meniscus is receding inside the capillary, the evaporation rate decreases continuously because the vapor has to diffuse over an increasing distance inside the capillary in agreement with previous reports in literature on Stefan's tube problem[75,76]. The evaporation rate $\frac{\mathrm{d}m}{\mathrm{d}t}$ in kg/s can be expressed from Fick's law[121] :

$$\frac{\mathrm{d}m}{\mathrm{d}t} = AD_v \frac{M_v}{RT} p_{vsat} \frac{(1-RH)}{\delta + \ell(t)}, \tag{2.1}$$

where $m = A\rho_w \ell(t)$ is the evaporated mass and $\ell(t)$ is the distance between the water-air meniscus on the evaporation side and the exit of the tube, see Fig. 2.2-a. A is the cross section surface area of the capillary, ρ_w is the density of liquid water, D_v is the vapor molecular diffusion coefficient ($D_v = 0.25 * 10^{-4}$ m^2/s[122]), R is the universal gas constant, M_v is the vapor molecular weight, T is the temperature, RH is the relative humidity of the ambiance, and p_{vsat} is the saturated vapor pressure at the considered temperature ($p_{vsat} = 2.3$ kPa). δ is defined as the vapor external transport length characterizing the vapor diffusive transport between the open end of the tube and the external air[123]. Our experiments differ from Stefan's situation due to the entrapped gas plug in the capillary. Nevertheless, as its volume remains constant, Eq. 2.1 is still valid. In this case, $\ell(t)$ can be obtained by equating the evaporation rate from Eq. 2.1 with $\frac{\mathrm{d}m}{\mathrm{d}t} = \rho_w A \frac{\mathrm{d}\ell}{\mathrm{d}t}$. Integrating the evaporation rate with the initial condition $\ell(t=0) = 0$ leads to the following equation for the evolution of the position of air/water meniscus on the evaporation side of the capillary (right meniscus in Fig. 2.2-a):

$$\ell(t) = \sqrt{\frac{2D_v M_v p_{vsat}(1-RH)}{\rho_w RT} t + \delta^2} - \delta \tag{2.2}$$

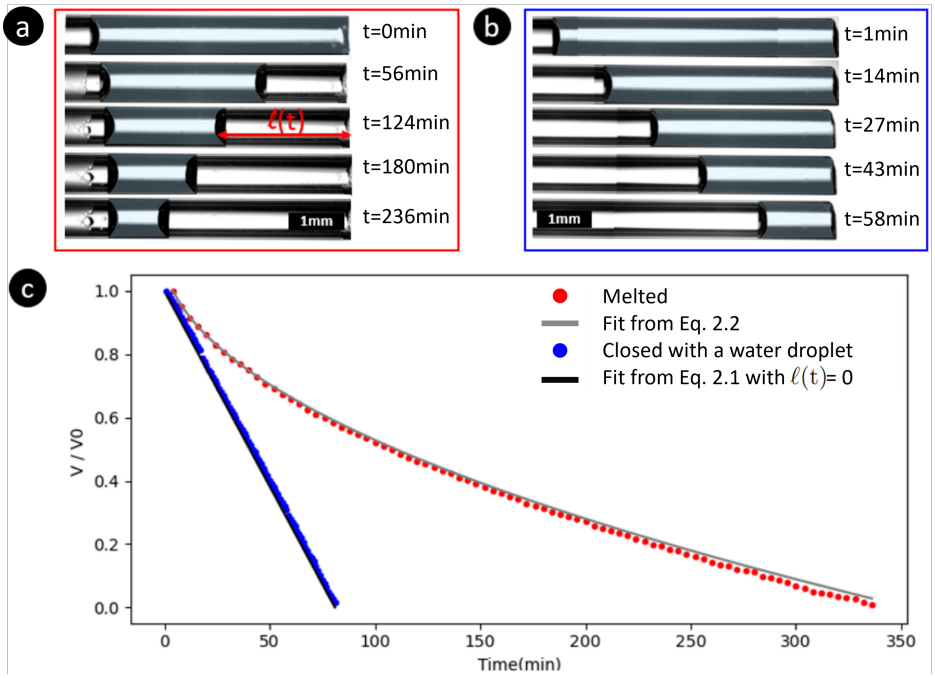

Figure 2.2. Microscope pictures of the drying of water (blue shaded zone on the pictures) in cylindrical capillaries with a melted end (a) and closed by a water droplet (b). In both configurations, the water is evaporating from the right. c) Volume of water plug in the capillary divided by the initial volume as a function of time (minutes). The red dots are experimental results for water evaporating in melted-end capillaries whereas the blue dots are the experimental results for capillaries closed by a water droplet. For the sake of clarity, only one example of each situation is plotted in the figure but four experiments have been performed for each situation.

Using $V(t) = V_0 - A * \ell(t)$ (where V_0 is the volume of water in the capillary at $t = 0$), we can predict the time evolution of liquid volume V and compare it with the experimental results shown by a solid-line in Fig. 2.2-c. δ is computed from Eq. 2.2 for every experiments performed and is found to be equal to $\delta = 0.30 \pm 0.06$ mm. This value is in line with the result reported in[78] where it is shown that δ is equal to $0.77d$ for a square tube, where d is the tube internal side length (in our case $0.77d = 0.385$ mm $\approx \delta_{exp}$). Thus the experimental data are in good agreement with the theoretical prediction of the Stefan model demonstrating that the evaporation rate is controlled by diffusion and is not affected by the entrapped gas plug.

Unexpectedly, in case (b), the volume of the water plug drops linearly with time. The evaporation rate is constant and is given by Eq. 2.1 with $\ell(t) = 0$ and $\delta \approx 200$ μm, as determined in Appendix 2.5.1. Moreover, performing the experiments with different geometries (round or square) does not affect the evaporation rate in contrast to the dead-end pore situation where the geometry can affect the receding meniscus and induce a much faster evaporation due to the liquid film flows in the corners of the square capillary[78,124] (see Appendix 2.5.2 for the experimental results with square capillaries). Experimentally, we can notice that fluid A enters the capillary (visible in Fig. 2.3) at the same volumetric rate as the evaporation rate. The volume of the gas plug inside the capillary remains thus constant during the whole drying. In order to keep the water meniscus pinned at the evaporation

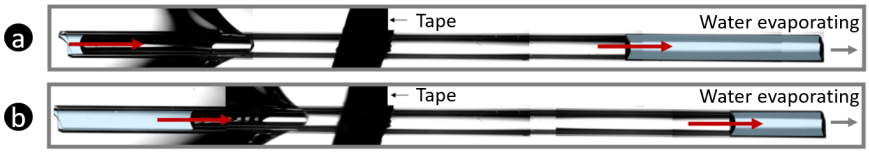

Figure 2.3. Microscope pictures of the full capillary of inner diameter 0.5 mm closed by a water droplet (right side) at $t = 0$ min (a) and $t = 43$ min (b). The blue shaded zones show the water evaporating from the right side and entering the capillary from the droplet on the left side.

side during the whole evaporation period, water must flow toward the exit of the capillary as the evaporation proceeds. It can be assumed that this flow results from the spontaneous imbibition of fluid A into the tube by capillarity as discussed in Chapter 1 and described by Washburn[125]. However as discussed in some detail in the Appendix 2.5.3, the spontaneous imbibition step of fluid A into the tube is very fast (less than 1 s for all the fluids tested) and stops very rapidly due the pressure build-up in the entrapped gas plug until a quasi-hydrostatic distribution of the fluids in the capillary is reached[126]. Evaporation is negligible during this fast transient step and fluid A penetration distance into the capillary during the spontaneous imbibition step is quite limited (a few tens of microns according to

the results reported in the Appendix 2.5.3).

The penetration of fluid A into the tube leads to an overpressure in the gas plug. Indeed, the hydrostatic equilibrium condition is that the pressure P_{Aeq} is uniform in fluid A entering the capillary. Thus, from Young –Laplace equation, the capillary pressure in fluid A is:

$$P_{cA} = P_g - P_{Aeq} = \frac{4\gamma_A cos\theta_2}{d} \tag{2.3}$$

where γ_A is fluid A surface tension and P_g is the pressure in the gas plug. For a tube of 0.5 mm in diameter and water as fluid A ($\theta_2 \approx 40°$) the overpressure in the tube is 450 Pa. We can verify if this is correct by determining the length of the gas plug from the ideal gas law:

$$\ell_g = z_2 - z_1 = (L - z_1(t=0)) * \frac{P_{atm}}{P_g} \tag{2.4}$$

In Fig. 2.3, $z_1(t=0) \approx 5$ mm and $L = 19.4$ mm the length of the capillary. This yields $\ell_g = 14.3$ mm according to equation 2.4 which is in very good agreement with Fig. 2.1 where $\ell_g \approx 14.2$ mm. Note that we have considered for this calculation that $P_{Aeq} \approx P_{atm}$. In fact, the pressure in fluid A at the entrance of the tube is slightly greater due to the weight of the liquid in the droplet above the tube entrance. The height of the droplet h is limited by gravity effect and is given by $h = 2\ell_{ca} sin(\frac{\theta_A}{2})$ where ℓ_{ca} is the capillary length[65] ($\ell_{ca} = 2.7$ mm for water). The corresponding additional hydrostatic pressure at the entrance of the tube can be estimated as $P_{Aeq} - P_{atm} \approx \rho_A g(h - \frac{d}{2})$. For $\theta_2 = 40°$ for instance, this gives $P_{Aeq} - P_{atm} = 18$ Pa, which is small compared to the capillary pressure ($P_{cA} = 450$ Pa). Considering this correction does not change the previous estimate, $\ell_g = 14.3$ mm.

In the long evaporation step that follows the very fast and limited imbibition step, the system operates with a quasi-static distribution of the fluids in the capillary. Nevertheless, a flow is induced in the entrapped water evaporating, the gas plug and fluid A (liquid plug) since the gas plug moves in direction of the pinned evaporative meniscus. This flow in entrapped water for round capillaries can be expressed using Poiseuille's law as

$$\frac{\mathrm{d}m}{\mathrm{d}t} = \rho_w A \frac{d^2}{32\mu_w} \frac{\Delta P_w}{z_1}, \tag{2.5}$$

where μ_W is the water dynamic viscosity. Applying this relationship at the beginning of the evaporation step, *i.e.* for $z_1 = 5$ mm, yields $\Delta P_w \approx 10^{-3}$ Pa, which is completely negligible compared to the capillary pressure (450 Pa). The pressure difference ΔP_w is the viscous pressure drop in the evaporating water plug resulting from the evaporation process. As a result, the water plug flows toward the entrance

of the capillary, where the evaporating meniscus remains pinned. The pressure in this water plug is slightly lower at the evaporating meniscus than at the left meniscus (Fig. 2.3). This implies that the meniscus curvature is less at the evaporating meniscus (roughly the liquid pressure in this water plug is $P_{w-left} \approx P_{atm}$ at the left meniscus whereas $P_{w-right} \approx P_{atm} - \Delta P_w$ at the right meniscus). Since ΔP_w is quite small compared to the maximum capillary pressure (450 Pa), the evaporating (right) meniscus is in fact almost flat, whereas the left meniscus is at maximum curvature (this is qualitatively visible in Fig. 2.3). Similarly, the fluid A volumetric flow rate q_v can be expressed as $q_v = \frac{1}{\rho_w}\frac{\mathrm{d}m}{\mathrm{d}t} = A\frac{d^2}{32\mu_A}\frac{\Delta P_A}{L-z_2}$. For $z_2 = L - 5$ mm (at the end of drying), this gives for water as fluid A a similar negligible pressure drop ΔP_A. The viscous pressure drop in the gas plug is even more negligible due to the much lower viscosity of air.

2.3.2 Transition from constant evaporation rate to diffusive evaporation period

2.3.2.1 Viscous dissipation in Fluid A

To evaluate the influence of fluid A viscosity on the drying regime of water, glycerol ($\mu = 1.4$ Pa.s) and PDMS ($\mu = 98$ Pa.s $\approx 10^5 \mu_{Water}$) are used as liquid reservoirs. Experimentally, the viscosity of fluid A does not seem to impact the drying kinetics: the water-air meniscus remains pinned at the exit of the capillary and drying proceeds with the same constant rate. However, the estimate of the pressure drop in fluid A toward the end of drying, *i.e.*

$$\Delta P_A = \frac{32\mu_A}{Ad^2} q_v (L - z_2) \tag{2.6}$$

gives for the most viscous fluid considered in the experiment (PDMS, $\mu_A = 98$ Pa.s) and for $L - z_2 = 5$ mm, $\Delta P_A = 96$ Pa, which is comparable to the capillary pressure ($P_{cA} = \frac{4\gamma_A cos\theta_2}{d} = 153$ Pa for PDMS with $\gamma_A = 20$ N.m^{-1} [127]). Thus, contrary to water for which the pressure variation in the gas plug is negligible, the pressure in the gas plug P_g decreases during the evaporation process when fluid A is very viscous, varying from $P_{atm} + P_{cA}$ to $P_{atm} + P_{cA} - \Delta P_A$.

Interestingly, it can be anticipated that if a larger initial volume of entrapped water evaporates in the capillary, a transition from a constant evaporation rate period to a diffusive evaporation period *i.e.* a transition from a air/water meniscus pinned at the evaporation side to a receding meniscus could be observed. For such a transition to occur the pressure in fluid A plug must become lower than the pressure $P_{atm} - P_{cw}$ at the air/water meniscus located in $z = 0$ (Fig. 2.1). Neglecting the viscous pressure drop in water plug, the pressure in the gas plug P_g is given by $P_g - P_{cw} = P_{atm} - P_{cw}$, which corresponds to $\Delta P_A = P_{cpdms}$. Solving equation 2.6 with $\Delta P_A = P_{cpdms}$ gives the distance $L - z_{2t}$ over which the fluid A

meniscus must flow in the tube before a transition from a constant evaporation rate period to a falling evaporation rate period could be observed. We introduced here z_{2t} the length z_2 for which the transition between the two regimes occurs. This gives $L - z_{2t} = Ca^{-1}d$, with d the capillary diameter and $Ca^{-1} = \frac{4\gamma_A cos\theta_2}{32\mu_A v_{ev}}$ where the evaporation velocity is given by $v_{ev} = \frac{1}{\rho_w A}\frac{\mathrm{d}m}{\mathrm{d}t}$. The dimensionless number Ca is the capillary number characterising the relative effects of viscous forces versus capillary forces. For the PDMS experiment, $Ca^{-1} \approx 16$. Thus, in the case of experiment with PDMS, $L - z_{2t} = 16d \approx 8$ mm. For the studied configuration, an initial water plug greater than about 8 mm should therefore be sufficient to observe the transition. In the case of porous media, it is well established that viscous effects induce the formation of a receding evaporation front in the material[111]. Although the situation is somewhat more complex in the presence of two liquids of different viscosity separated by a gas plug, the simple configuration studied here indicates that a similar transition can be observed in a simple model pore by playing with the viscosity of fluid A acting as liquid plug.

As described in Appendix 2.5.4, the impact of the viscosity can be considered in a model aiming at predicting the drying kinetics. This model indicates that the transition can be also expected by reducing the tube diameter instead of modifying the initial length of the water plug, keeping all other parameters the same. This results from the fact that the viscous pressure drop in the PDMS plug varies as d^{-2}. Reducing the tube diameter has also an impact on the evaporation velocity since $\delta \propto d$. Taking into account this impact, by reducing the tube diameter from 500 μm to 300 μm, one obtains $Ca^{-1} \approx 9.6$. Thus $L - z_{2t} \approx 9.6d = 2.88$ mm and an initial plug shorter than the ones in the previous experiments should be sufficient to observe the transition between the two evaporative regimes with a tube of 300 μm in diameter. To confirm the relevance of this model and the associated predictions, an experiment with a longer capillary of length $L = 31.6$ mm and diameter 300 μm is performed with a longer initial water plug ($z_1(t = 0) = 10.8$ mm). This leads to the results depicted in Fig. 2.4 and Fig. 2.5-a. As expected a transition is obtained between a constant evaporation rate period (CRP) and a falling evaporation rate period (FRP). In Fig. 2.4, the CRP corresponds to the initial linear evolution of $z_1(t)$ whereas the FRP corresponds to the period that follows when the absolute value of the slope $|\frac{\mathrm{d}z_1}{\mathrm{d}t}|$ is smaller. For these experimental conditions in the CRP, the evaporation velocity determined from Eq. 2.1 with $\ell(t) = 0$ (pinned meniscus) is 1.63×10^{-6} m/s, which is quite comparable to the experimental value $-\frac{\mathrm{d}z_1}{\mathrm{d}t} = 1.65 \times 10^{-6}$ m/s obtained from a fit of the experimental data in the CRP. The inverse of the capillary number for this experiment is $Ca^{-1} = 13.4$, which gives $L - z_{2t} = 4$ mm. Thus, the CRP/FRP transition is expected when the water plug size is reduced by 4 mm, *i.e.,* when $z_1 = z_{1t} = 6.8$ mm. As can be seen from Fig. 2.4, this prediction is in good agreement with the experimental data.

However, as can be seen from Fig. 2.4, the model presented in Appendix 2.5.4 for determining the drying kinetics over both the CRP and the FRP leads to a

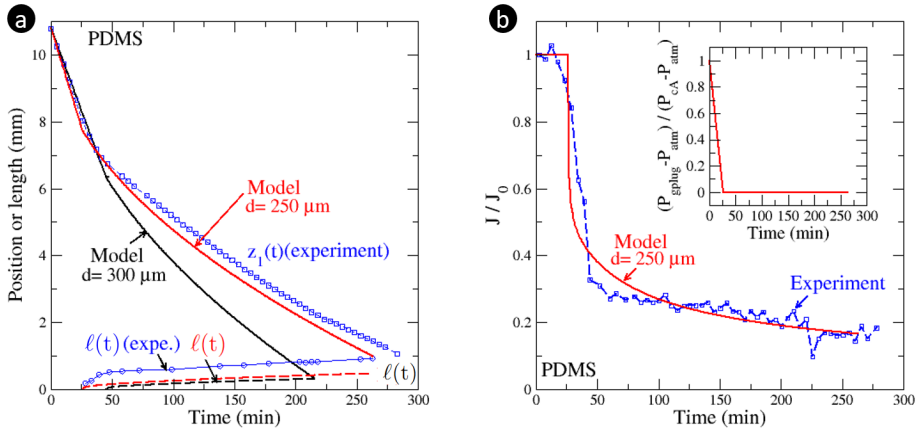

Figure 2.4. a) Impact of fluid A penetration on the drying kinetics for configuration (b) of Fig. 2.1. Refer to Fig. 2.1 for the definition of z_1 and z_2 and to Fig. 2.2-a for the definition of ℓ. b) Drying kinetics ($J = -\frac{\mathrm{d}m}{\mathrm{d}t}$ is the evaporation rate, J_0 is the evaporation rate when the evaporative meniscus is pinned at the evaporation exit). The inset shows the pressure variation in the gas plug computed from the model in Appendix 2.5.4. The experimental results are plotted in blue whereas the results obtained with the model are shown in red for capillaries of $d = 250$ μm and in black for capillaries of $d = 300$ μm.

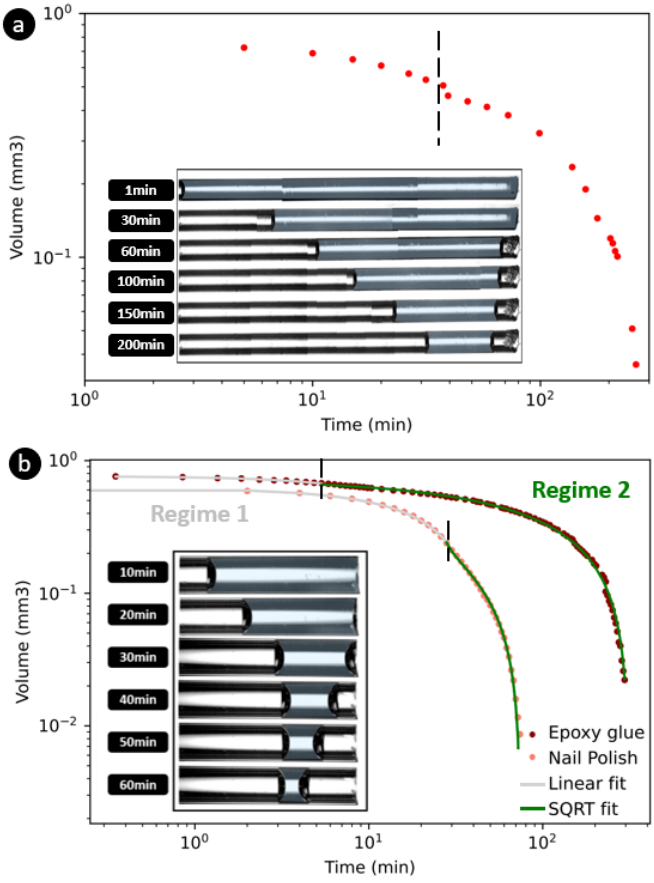

Figure 2.5. Volume of entrapped water evaporating in a cylindrical capillary plotted as a function of time. In a), the capillary ($d = 0.3$ mm) is closed from the left side with PDMS and the two evaporative regimes can be clearly identified. In b), the capillary ($d = 0.5$ mm) is closed with a drop of nail polish or of epoxy glue: the change in the drying kinetics of water indicates the phase transition of the nail polish and epoxy glue from their liquid states to their solid-like states. The microscope pictures show the drying of water in the capillary closed by a droplet of nail polish.

faster drying. This discrepancy can be related to the prediction of the dry region size at the tube end during the FRP, *i.e.,* the distance over which the evaporative meniscus recedes into the tube. Although the length ℓ plotted in Fig. 2.4 does not have exactly the same definition in the experiment (as shown in Fig. 2.2-a, ℓ is the distance between the meniscus and the tube end measured from the images) and in the model where ℓ is determined from Eq. 2.1 (see Supporting Information), the model predicts a shorter receding distance. Since ℓ is not large compared to the external mass transfer characteristic length δ, the evaporation rate is highly sensitive to the value of δ. Since the model depends on several physical and geometrical parameters, the question arises as to whether the discrepancy is due to questionable values of parameters or to questionable assumptions or approximations in the modelling. We have tested the model sensitivity to several physical parameters (liquid A viscosity and surface tension, contact angles, etc). Increasing the PDMS contact angle to 35° for instance slightly improves the model prediction. Increasing the PDMS viscosity has also a favorable impact but the discrepancy remains noticeable unless a significantly greater viscosity value than the one corresponding to the used PDMS is considered (*i.e.,* $\mu_A = 98$ Pa.s). Also, we have considered the situation where the water wettability is different in the tube end region compared to deeper inside the tube. The conclusion is that the most sensitive parameter is the tube diameter (again because the viscous pressure drop for a given velocity varies as d^{-2}).

As illustrated in Fig. 2.4-a, considering a diameter of 250 μm for instance leads to a significantly better agreement between the model and the experimental data. Also as shown in Fig. 2.4-b, the agreement between the model and the experiment is quite good as regards to the evaporation rate (determined for the experiment using a simple finite difference from the experimental data, *i.e.* $\frac{\mathrm{d}m}{\mathrm{d}t} = -\rho_w A \frac{z_1(t_{i+1}) - z_1(t_i)}{t_{i+1} - t_i}$). Fig. 2.4-b (inset) also shows the variation of the pressure in the gas plug as predicted by the model. The pressure decreases linearly from $P_{atm} + P_{cA}$ to P_{atm} during the CRP and stays constant and equal to P_{atm} during the FRP. Further investigations are desirable to better understand why the model leads to a faster drying when setting diameter of tube 300 μm, whereas the agreement is much better when a value of 250 μm is considered. Since the meniscus receding distance is small (900 μm which is about three time the tube diameter in the experiment at the end of drying), *i.e.* not very large compared to the external mass transfer characteristic length ($\delta \approx 180$ μm), the details of the meniscus displacement in the tube end region matters. Thus, perhaps a more detailed investigation of the meniscus depinning in this region during the CRP/FRP transition could help explain the discrepancy with the experimental data. In any case, the model consistently predicts a drying kinetics in two main evaporation periods due to the viscous effects when $z_1(t = 0) > Ca^{-1}d$.

2.3.2.2 Solidification of fluid A

Finally, the impact of fluid A properties on drying kinetics can be further illustrated by considering fluids which can undergo a phase transition from liquid to solid either by drying or temperature change. This is notably the case of adhesives which are used in civil engineering to fix two materials together (tiles on a wall for example). Moreover, glues have been frequently used in previous experiments to close capillaries and induce unidirectional drying[115]. We have performed experiments with nail polish and epoxy glue which both solidify during their drying. As it can be seen in Fig. 2.5-b, two different evaporation regimes can be observed for the entrapped water. During the first period, the meniscus of the entrapped water is pinned at the exit of the tube and the fluid A, still liquid, enters the capillary from the other side. This regime is effectively described by Eq. 2.1 when setting $\ell(t) = 0$. In those situations the evaporation rate is $\frac{1}{\rho(1-RH)}\frac{\mathrm{d}m}{\mathrm{d}t} = (4.49 \pm 0.18) * 10^{-4}$ mm^3/s as described above. As time passes, fluid A solidifies and cannot advance in the capillary anymore. This phase transition leads to the second evaporation regime during which the air-water meniscus recedes inside the capillary. The transition between the two evaporative regimes is therefore a clear indication of the solidifying time of the glue used as liquid plug to close the capillary.

2.4 Discussion and conclusion

We have shown that the dynamics of unidirectional drying of water in the presence of an entrapped gas plug in a single capillary are strongly dependent on whether the end of the capillary is connected to a liquid reservoir or clogged with a solid material. Contrary to the well-known case of the Stefan tube drying, evaporation can lead to capillary pumping when the round capillary is connected to a liquid reservoir and a much faster constant rate evaporation. In this configuration, the drying regime is not affected by the geometry of the pore *i.e.* the shape of the tube cross-section. If the liquid closing the capillary is sufficiently viscous, a transition from a constant rate evaporation regime to a diffusive regime can also be observed when the tube diameter and the size of the entrapped gas plug are sufficiently small. Finally we studied the influence of solidifying glues on the drying of capillaries partially filled with water. The use of such glues to seal capillaries can lead to drying behavior with two periods: a first period where the drying rate is constant and some glue enters the capillary, followed by a second diffusive regime once the glue is solidified. Such behaviours remain relevant in situations where soils or porous materials in general are connected to liquid reservoir or materials which can solidify (or gelify) over time.

2.5 Appendix

2.5.1 Determination of δ in configuration (b)

In configuration (b) in Fig. 2.2, the volume of the water plug drops linearly with time and the evaporation rate is constant. As the water evaporates at the entrance of the capillary during the whole drying, it is possible to determine the value of the external diffusive length δ using Fick's law.

$$\frac{\mathrm{d}m}{\mathrm{d}t} = AD_v \frac{M_v}{RT} p_{vsat} \frac{1 - RH}{\delta} \tag{2.7}$$

The diffusive length is extracted from every experiment and is equal to $\delta = 195 \pm 12$ μm which is in the same range as in configuration (a). The slightly smaller value found here can be qualitatively explained by the fact that the external transfer is slightly different when the meniscus is right at the entrance of the tube and when the meniscus in deeper inside the tube due to the difference in the structure of the local vapor partial pressure distribution in the tube exit region (the local evaporation flux is expected to be more uniform over the tube entrance when the meniscus is inside the tube compared to the case of a meniscus located right at the tube entrance. In the latter case, a greater local flux at the tube end periphery is expected, somewhat similarly to the local evaporation flux distribution over an evaporative flat droplet). Nevertheless, these considerations would deserve to be explored in more details from numerical simulations, in the spirit of the results shown in[128] , where the evaporation rate from a flat meniscus at a channel end is compared to the one obtained when the meniscus has partially receded into the channel.

2.5.2 Results in square capillaries

Fig. 2.6 shows the results for configuration (a) and configuration (b) with square capillaries. In situation (a) where the capillary is closed by a melted plug, the evaporative meniscus recedes in the capillary and some corner flows are forming on the side of the capillary as described in the litterature[78,123,124,129]. This leads to a constant rate evaporation due to the presence of corner flows. In situation (b), as for round capillaries, the meniscus remains pinned at the evaporative side and one CRP is also observed until the end of the drying. Thus, performing the experiments with different geometries (round or square) does not affect the evaporation regimes. We can nevertheless notice that the evaporation rate is higher for situation (b) ($1.8 * 10^{-2}$ mm^3/min) than for situation (a) ($1.46 * 10^{-2}$ mm^3/min). This can be explained by the fact that the evaporation surface is higher in situation (b) compared to situation (a) where water evaporates mainly at the tip of the fingers[78,111].

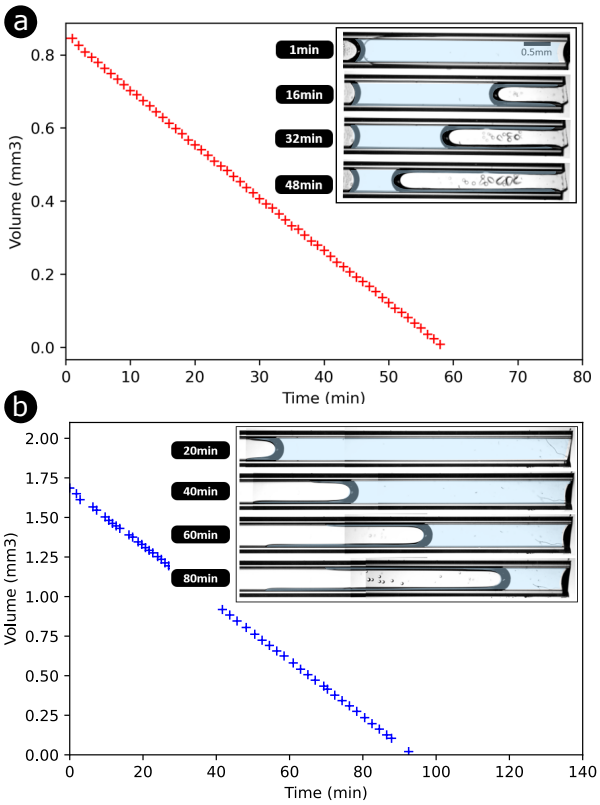

Figure 2.6. Drying of water (highlighted in blue) in square capillaries melted on one side (a) ($\frac{\mathrm{d}V}{\mathrm{d}t} = 1.46 * 10^{-2}$ mm^3/min) or closed by a water droplet (b) ($\frac{\mathrm{d}V}{\mathrm{d}t} = 1.8 * 10^{-2}$ mm^3/min).

	ρ_A (k/m^3)	γ_A (N/m)	θ_A (°)	μ_A (Pa.s)
water	1000	$72 * 10^{-3}$	40	10^{-3}
Glycerol	1260	63.4	10	1.5
PDMS[127]	965	20	16	98

Table 2.1. Physical properties of water, glycerol and PDMS used in the computations

2.5.3 Spontaneous imbibition step

In configuration (b), the very fast spontaneous imbibition period occurring when the capillary is connected to the droplet of fluid A can be analyzed using a classical Washburn model combined with the consideration of the pressure build-up in the gas plug and inertial effects in the liquid[126,130]. The equation governing the position of fluid A meniscus can be expressed as[126]:

$$\rho_A(\frac{\mathrm{d}\ell_A}{\mathrm{d}t})^2 = P_{cA} - \frac{32\mu_A}{d^2}\ell_A\frac{\mathrm{d}\ell_A}{\mathrm{d}t} + P_{atm}(1 - \frac{L - z_1}{L - z_1 - \ell_A}) \tag{2.8}$$

where $\ell_A = L - z_2$ is the position of fluid A meniscus measured from the capillary left end (Fig. 2.1), ρ_A is fluid A density and $P_{cA} = \frac{4\gamma_A cos\theta_A}{d}$. The properties for the three liquids considered are given in Table 2.1.

Solving numerically Eq. 2.4, for $L = 19.4$ mm, $z_1 = 5$ mm leads to the results shown in Fig. 2.7. As can be seen, the greater the viscosity, the longer is the imbibition period (1000 times longer with PDMS compared to water for instance). Nevertheless, the imbibition period is very short, less than 1 second, even for the most viscous fluid tested. Interestingly, the forces controlling the spontaneous imbibition differs depending on the fluid. For water, the less viscous fluid, the imbibition is dominated by the capillary and inertial forces (the viscous term $\frac{32\mu_A}{d^2}\ell_A\frac{\mathrm{d}\ell_A}{\mathrm{d}t}$ can be neglected in Eq. 2.8) except at the very end when the meniscus velocity approaches zero). By contrast, the inertial effects (*i.e.* the term $\rho_A(\frac{\mathrm{d}\ell_A}{\mathrm{d}t})^2$ in Eq. 2.8) are negligible for the most viscous fluid (PDMS). The imbibition is controlled by the capillary and viscous effects. The situation for the third fluid, glycerol, is intermediate. Inertial effects are dominant in a first period and the viscous effects become gradually more and more important as the hydrostatic equilibrium is approached.

The penetration distance is shorter for the most viscous fluid but is quite short for the three fluids, on the order of a few tens of micrometers. The pressure in the gas plug is computed applying the ideal gas law as $P_g(t) = P_{atm}\frac{L - z_1(t=0)}{L - z_1(t=0) - \ell_A(t)}$. The maximum pressure in the gas plug (which corresponds to the plateaus in Fig. 2.7) is given by $P_g \approx P_{atm} + P_{cA}$, neglecting the slight overpressure due to the height of the liquid in the droplet.

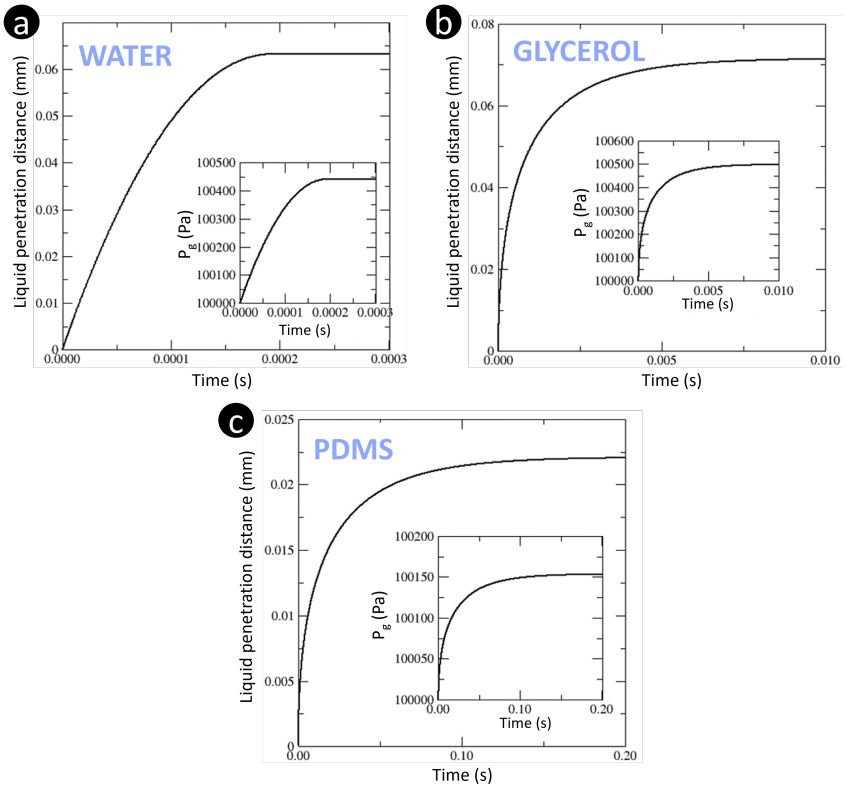

Figure 2.7. Evolution of fluid A penetration distance ℓ_A during the period of spontaneous imbibition for water (a), glycerol (b) and PDMS (c). The insets show the pressure evolution in the gas plug.

2.5.4 Drying with viscous effect (configuration (b) in Fig. 2.1)

The drying rate is expressed using the following equation:

$$\frac{\mathrm{d}m}{\mathrm{d}t} = AD_v \frac{M_v}{RT} p_{vsat} \frac{1 - RH}{\delta + \ell(t)} \tag{2.9}$$

Neglecting the viscous pressure drop in the liquid water plug and the gas plug and considering the viscous pressure drop in the region of the tube occupied by fluid A, the pressure in the water right behind the evaporative meniscus can be expressed as:

$$P_w = P_{atm} - \Delta P_A + P_{cA} - P_{cw} \tag{2.10}$$

Where $P_{cA} = \frac{4\gamma_A cos\theta_A}{d}$, $P_{cw} = \frac{4\gamma_w cos\theta_w}{d}$, $\Delta P_A = \frac{32\mu_A}{d^2 v_{ev}}(L - z_2)$ and v_{ev} is the evaporation velocity. The pressure jump P_{cem} at the evaporative meniscus is then given by,

$$P_{cem} = P_{atm} - P_w = \Delta P_A - P_{cA} + P_{cw} \tag{2.11}$$

The evaporative meniscus is pinned at the tube end as long as $P_{cem} < P_{cw}$. This corresponds to a first period where the evaporation rate is constant. The evolution of z_2 in this period is given by $\frac{dz_2}{dt} = \frac{dz_1}{dt} = -v_{ev}$. As fluid A penetrates further in the tube, *i.e.* as the penetration distance $(L - z_2)$ increases, the viscous pressure drop increases until $P_{cem} = P_{cw}$. According to Eq. 2.11, this corresponds to $(L - z_{2t})$ given by solving the equation $\Delta P_A P_{cA} = 0$. Thus $z_{2t} = L - \frac{d^2}{32\mu_A v_{ev}} \frac{4\gamma_A cos\theta_A}{d}$ or $z_{2t} = L - Ca^{-1}d$ with $Ca^{-1} = \frac{4\gamma_A cos\theta_A}{32\mu_A v_{ev}}$. When this situation is reached, the evaporative meniscus starts receding into the tube. In the second period, the pressure in the gas plug is imposed by the curvature of the water menisci in the tube. Therefore, $P_g = P_{atm}$. As a result, the viscous volumetric flow rate q_A in fluid A is given by:

$$q_A = -A\frac{\mathrm{d}z_2}{\mathrm{d}t} = A\frac{d^2}{32\mu_A}\frac{P_{cA}}{L - z_2} \tag{2.12}$$

This equation gives the position of fluid A meniscus as a function of time in the second period, namely:

$$z_2(t) = L - \sqrt{(L - z_{2t})^2 + \frac{2d^2 P_{cA}}{32\mu_A}(t - t_t)}, \qquad (t \geq t_t) \tag{2.13}$$

where t_t is the time marking the transition between the constant evaporation rate period and the falling evaporation rate period. This time is given by the equation$(L - z_{2t} = v_{ev} t_t)$ where $v_{ev} = \frac{1}{\rho_w} D_v \frac{M_v}{RT} p_{vsat} \frac{(1-RH)}{\delta}$ according to Eq. 2.9.

We have still two unknowns to be determined during the second period: $z_1(t)$ and $\ell(t)$ where $\ell(t)$ is the position of the evaporative meniscus in the tube. Expressing

that the evaporation corresponds the water mass loss of the water plug yields:

$$\frac{\mathrm{d}(z_1 - \ell)}{\mathrm{d}t} = \frac{1}{\rho_w A}\frac{\mathrm{d}m}{\mathrm{d}t} = \frac{1}{\rho_w} D_v \frac{M_v}{RT} p_{vsat} \frac{1 - RH}{\delta + \ell(t)} \tag{2.14}$$

In the considered experiments, the pressure variation in the gas plug remains small compared to the atmospheric pressure. As the result, the gas plug length variations are small. An approximation consists in neglecting these variations, which allows to compute $z_1(t)$ from the relationship,

$$z_1(t) = z_2(t) - L + z_1(t = 0) \tag{2.15}$$

noting that the initial imbibition distance is very small, *i.e.* $z_2(t) \approx L$. The method of solution then consists in determining $z_2(t)$ for the next time step from Eq. 2.13. Then $z_1(t)$ is determined from Eq. 2.15 whereas ℓ is computed from Eq. 2.14 expressed as $-\frac{\mathrm{d}\ell}{\mathrm{d}t} = \frac{1}{\rho_w} D_v \frac{M_v}{RT} p_{vsat} \frac{1-RH}{\delta+\ell(t)} - \frac{\mathrm{d}z_1}{\mathrm{d}t}$ using a simple Euler scheme.